


Article

The Link between Cytogenetics/Genomics and Imaging Patterns of Relapse and Progression in Patients with Relapsed/Refractory Multiple Myeloma: A Pilot Study Utilizing 18F-FDG PET/CT

Xiang Zhou ¹, Alexander Dierks ^{2,3}, Olivia Kertels ⁴, Samuel Samnick ², Malte Kircher ^{2,3}, Andreas K. Buck ², Larissa Haertle ¹, Sebastian Knorz ¹, David Böckle ¹, Lukas Scheller ¹, Janin Messerschmidt ¹, Mohammad Barakat ¹, Marietta Truger ⁵, Claudia Haferlach ⁵, Hermann Einsele ¹, Leo Rasche ¹, K. Martin Kortüm ¹  and Constantin Lapa ^{2,3,*}

¹ Department of Internal Medicine II, University Hospital of Würzburg, Oberdürrbacher Street 6, D-97080 Würzburg, Germany; zhou_x@ukw.de (X.Z.); haertle_l@ukw.de (L.H.); knorz_s@ukw.de (S.K.); boeckle_d@ukw.de (D.B.); scheller_l@ukw.de (L.S.); Messerschm_j@ukw.de (J.M.); barakat_m@ukw.de (M.B.); Einsele_H@ukw.de (H.E.); rasche_l@ukw.de (L.R.); Kortuem_M@ukw.de (K.M.K.)

² Department of Nuclear Medicine, University Hospital of Würzburg, D-97080 Würzburg, Germany; dierks_a@ukw.de (A.D.); samnick_S@ukw.de (S.S.); malte.kircher@uk-augsburg.de (M.K.); buck_a@ukw.de (A.K.B.)

³ Nuclear Medicine, Medical Faculty, University Hospital of Augsburg, D-86156 Augsburg, Germany

⁴ Department of Diagnostic and Interventional Radiology, University Hospital of Würzburg, D-97080 Würzburg, Germany; kertels_o@ukw.de

⁵ Munich Leukemia Laboratory, D-81377 Munich, Germany; marietta.truger@mll.com (M.T.); claudia.haferlach@mll.com (C.H.)

* Correspondence: Constantin.Lapa@uk-augsburg.de

Received: 30 July 2020; Accepted: 21 August 2020; Published: 24 August 2020



Abstract: Utilizing 18F-fluorodeoxyglucose (18F-FDG) positron emission tomography (PET)/computed tomography (CT), we performed this pilot study to evaluate the link between cytogenetic/genomic markers and imaging patterns in relapsed/refractory (RR) multiple myeloma (MM). We retrospectively analyzed data of 24 patients with RRMM who were treated at our institution between November 2018 and February 2020. At the last relapse/progression, patients had been treated with a median of three (range 1–10) lines of therapy. Six (25%) patients showed FDG avid extramedullary disease without adjacency to bone. We observed significantly higher maximum standardized uptake values (SUV_{max}) in patients harboring del(17p) compared with those without del(17p) ($p = 0.025$). Moreover, a high SUV_{max} of >15 indicated significantly shortened progression-free survival (PFS) ($p = 0.01$) and overall survival (OS) ($p = 0.0002$). One female patient exhibited biallelic TP53 alteration, i.e., deletion and mutation, in whom an extremely high SUV_{max} of 37.88 was observed. In summary, this pilot study suggested a link between del(17p)/TP53 alteration and high SUV_{max} on 18F-FDG PET/CT in RRMM patients. Further investigations are highly warranted at this point.

Keywords: radiogenomics; 18F-FDG PET/CT; multiple myeloma; relapse; progression; pattern

1. Introduction

Multiple myeloma (MM) represents the second most common hematological malignancy in adults [1]. In MM, functional imaging methods, such as diffusion-weighted (DW) magnetic resonance imaging (MRI) and 18F-fluorodeoxyglucose (18F-FDG) positron emission tomography (PET)/computed

tomography (CT), can display diffuse growth patterns, focal lesions, and extramedullary disease (EMD) of patients (Figure 1). In the current consensus recommendation by the International Myeloma Working Group (IMWG), 18F-FDG PET/CT is considered a valuable tool for the visualization of disease activity in both newly diagnosed (ND) and relapsed/refractory (RR) MM patients [2]. 18F-FDG PET/CT has also been used for the prediction of survival outcome in MM patients treated with allogeneic stem cell transplant [3].

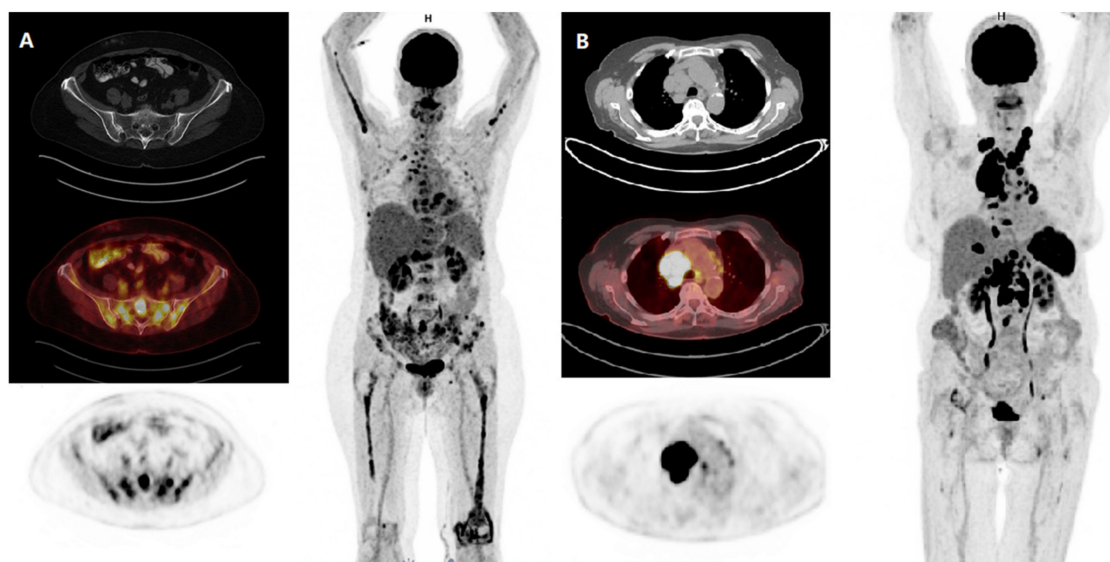


Figure 1. 18F-FDG PET/CT in two patients with multiple myeloma. 18F-FDG PET/CT demonstrates FDG avid (A) medullary lesions (pelvis, spine, both humeri and both femurs) and (B) extramedullary manifestations (mediastinal lymph nodes) in patients with multiple myeloma. 18F-FDG, 18F-fluorodeoxyglucose; PET, positron emission tomography; CT, computed tomography.

To date, there are also a few studies evaluating the association between cytogenetic abnormalities and imaging patterns in newly diagnosed MM (NDMM). Recently, adverse cytogenetics, such as $\text{del}(17p)$, $\text{gain}(1q21)$, and $\text{t}(4;14)$, have been reported to be enriched in NDMM patients with diffuse infiltration pattern in DWMRI C [4]. Moreover, $\text{del}(17p)$, $\text{gain}(1q21)$, and gene expression profiling (GEP)-based high-risk disease are more frequent in NDMM patients with at least three large focal lesions $>5 \text{ cm}^2$ [5]. Furthermore, McDonald et al. reported that total lesion glycolysis (TLG) $>620 \text{ g}$ and metabolic tumor volume (MTV) $>210 \text{ cm}^3$ indicated a significantly inferior progression-free survival (PFS) and overall survival (OS) of myeloma patients [6]. However, it has been less extensively investigated if imaging patterns of relapse and progression correlate with cytogenetic/genomic markers in RRMM. Therefore, we performed this pilot study in RRMM utilizing 18F-FDG PET/CT.

The aim of the current study was to evaluate the potential link between imaging patterns of relapse or progression and cytogenetic/genomic characteristics in RRMM and to generate hypotheses for further investigations.

2. Methods

2.1. Patient Population

This was a single-center retrospective cohort study. We identified 24 patients who were treated for RRMM between November 2018 and February 2020. RRMM was defined as per current IMWG criteria [7]. At the last relapse/progression, we simultaneously performed a bone marrow biopsy plus an 18F-FDG-PET/CT prior to therapy initiation in all patients. Patients with active second tumor were excluded from the analysis. Patients' characteristics, including time point of diagnosis, MM subtype, prior lines of therapy, and drug resistance status, were collected for the analysis of imaging

data (PET/CT scans and DWMRI if available). In addition, patterns of relapse or disease progression were noted (presence of extramedullary disease, serological activity, bone marrow infiltration rate, cytogenetics, and genomic data). All procedures were performed in accordance with national ethical standards and with the current version of the Declaration of Helsinki.

2.2. Imaging Analysis, Cytogenetics, and Genomic Data

We assessed the numbers of medullary and extramedullary sites, maximum standardized uptake value (SUV_{max}) of lesions, and the localization of the largest and “hottest” lesion. Correlation with DWMRI was performed in patients with available imaging. More details of 18F-FDG PET/CT image acquisition and imaging analysis are available in the Supplementary Methods.

Cytogenetic and genomic analyses were performed using bone marrow materials collected at the last relapse or progression. Cytogenetics was analyzed by fluorescence in situ hybridization (FISH) on CD138 purified cells. High-risk cytogenetics was defined according to the revised international staging system (R-ISS) for MM, i.e., del(17p), t(4;14), and t(14;16) [8]. Structural variations (SV), copy number variations (CNV), and point mutations were available from whole-genome sequencing (WGS) on CD138 purified cells in nine cases. More details are available in the 8F-FDG PET/CT image acquisition and imaging analysis are available in the Supplementary Methods or upon reasonable request.

2.3. Statistical Analysis

We summarized patients’ characteristics as absolute number and percentage or as median and range if not otherwise stated. Two-tailed Mann–Whitney U test was used to compare the SUV values in different subgroups. We used Kaplan–Meier methods to analyze the survival outcome of the patients. A univariate log-rank test was used to compare the survival curves in different groups. These analyses were performed with GraphPad Prism 5.0. A *p*-value of <0.05 was considered statistically significant.

3. Results

3.1. Patients’ Characteristics

All 24 patients suffered from relapse or progression of MM at the time point of bone marrow biopsy and 18F-FDG-PET/CT, which were performed prior to therapy initiation. Overall, 58% of the patients (*n* = 14) were male, and the median age at the last relapse/progression was 68 (range 46–81) years. The median time between diagnosis of MM and the last relapse/progression was 62 (range 17–192) months. Our cohort was highly pretreated with a median of three (range 1–10) prior lines of therapy. Most patients (*n* = 23, 96%) underwent high-dose melphalan and autologous, and three (13%) patients also allogeneic stem cell transplant (SCT). All patients (100%) had received prior bortezomib, and ten of them (42%) additional carfilzomib treatment. Lenalidomide, pomalidomide, and thalidomide were administered in 20 (83%), seven (29%), and three (13%) patients, respectively. Daratumumab was given in 13 (54%) patients, and two (8%) patients received elotuzumab. Eight (33%), nine (38%), 14 (58%), six (25%), and 11 (46%) patients were bortezomib, carfilzomib, lenalidomide, pomalidomide, and daratumumab refractory, respectively, and three (13%) patients were penta-refractory (bortezomib, carfilzomib, lenalidomide, pomalidomide, and daratumumab). Moreover, one (4%) and two (8%) patients received B-cell maturation antigen (BCMA)-targeted chimeric antigen receptor (CAR) T-cell therapy and bispecific antibody within clinical trials, respectively.

At the initial diagnosis of MM, all patients (100%) had measurable M component in serum, and primary EMD was present in five (21%) patients. In addition, one (4%) patient suffered from primary plasma cell leukemia (PCL) with $19.3 \times 10^3/\mu\text{L}$ circulating plasma cells in peripheral blood at diagnosis. Patients’ characteristics and treatment-related data are summarized in Table 1.

Table 1. Patients' characteristics.

Parameter	Number
Patients, <i>n</i>	24
Gender, <i>n</i> (%)	
Male	14 (58)
Female	10 (42)
Age at the last relapse/progression, median (range), years	68 (46–81)
Subtype, <i>n</i> (%)	
IgG	16 (67)
IgA	7 (29)
LC	1 (4)
ISS Stage, <i>n</i> (%)	
I	9 (37)
II	5 (21)
III	5 (21)
NA	5 (21)
Cytogenetics, <i>n</i> (%)	
High-risk	8 (33)
Standard-risk	15 (63)
NA	1 (4)
t(4;14)	
Yes	5 (21)
No	18 (75)
NA	1 (4)
t(14;16)	
Yes	1 (4)
No	19 (79)
NA	4 (17)
del(17p)	
Yes	4 (17)
No	19 (79)
NA	1 (4)
gain(1q21)	
Yes	10 (42)
No	13 (54)
NA	1 (4)
EMD at diagnosis, <i>n</i> (%)	
Yes	5 (21)
No	19 (79)
Prior lines of therapy, <i>n</i> (%)	
2–1 month	9 (38)
4–3 month	7 (29)
≥5	8 (33)
Prior treatments, <i>n</i> (%)	
PIs	
Bortezomib	24 (100)
Carfilzomib	10 (42)
IMiDs	
Lenalidomide	20 (83)
Pomalidomide	7 (29)
Thalidomide	3 (13)

Table 1. Cont.

Parameter	Number
Monoclonal antibodies	
Daratumumab	13 (54)
Elotuzumab	2 (8)
SCT	
Prior autologous SCT	23 (96)
Prior allogenic SCT	3 (13)
BCMA-directed novel immunotherapies within clinical trials	
Bispecific antibody	2 (8)
CAR-T-cell	1 (4)
Drug resistance, n (%)	
Bortezomib	8 (33)
Carfilzomib	9 (38)
Lenalidomide	14 (58)
Pomalidomide	6 (25)
Daratumumab	11 (46)

BCMA—B-cell maturation antigen; CAR—chimeric antigen receptor; EMD—extramedullary disease; IMiDs—immunomodulatory drugs; ISS—the multiple myeloma international staging system; LC—light chain; MM—multiple myeloma; NA—not available; PIs—proteasome inhibitors; SCT—stem cell transplant.

3.2. Patterns of Relapse and Progression

Fourteen (58%) patients progressed on or within 60 days of receiving the last treatment, and we then started a new line of therapy. The other ten (42%) patients relapsed from partial remission (PR) or better, and the median time after the last treatment was 10 (range 3–29) months in these ten patients. The majority of the patients ($n = 22$, 92%) presented an increasing M component in serum, while two (8%) of them showed no serological activity but EMD. Four (17%) patients had a bone marrow infiltration of <10%. The lactate dehydrogenase level was elevated in seven (29%) patients. Thirteen (54%) patients showed a β 2-microglobulin level of ≥ 3.5 mg/L.

As demonstrated in 18F-FDG PET/CT, which was performed at the last relapse/progression, the vast majority of the patients ($n = 23$, 96%) exhibited medullary lesions. Six (25%) patients suffered from true EMD without adjacency to bone. The lymph node was the most common localization of EMD (3/6). One and two out of six patients had EMD in soft tissue and parenchymal organ, respectively. At the time point of the last relapse/progression, the one patient who had primary PCL at the first diagnosis developed soft tissue EMD and serological progression. However, PCL was no longer present in this patient. Among all medullary and extramedullary lesions, the median SUV_{max} was 8.15 (range 3.81–39.14). In two (8%) patients, EMD represented the overall hottest lesion. At the last relapse/progression, both 18F-FDG PET/CT scan and DWMRI were available in six (25%) patients. Notably, in two out of six patients, we observed more diffusion-weighted imaging (DWI) positive lesions in DWMRI compared to 18F-FDG PET/CT scans. Patterns of relapse and progression are summarized in Table 2.

Table 2. Patterns of relapse and progression.

Parameter	Number
Patients, n	24
Serological activity, n (%)	
Yes	22 (92)
No	2 (8)
Bone marrow infiltration, n (%)	
<10%	4 (17)
$\geq 10\%$	17 (71)
NA	3 (12)

Table 2. Cont.

Parameter	Number
Laboratory parameters, n (%)	
eGFR, mL/min (CKD-EPI), median (range)	70 (34–98)
≥50 mL/min	18 (75)
<50 mL/min	6 (25)
Calcium, mmol/L, median (range)	2.5 (2.0–2.3)
≥2.5 mmol/L	0 (0)
<2.5 mmol/L	24 (100)
LDH, U/L, median (range)	197 (107–711)
≥250 U/L	7 (29)
<250 U/L	17 (71)
Hemoglobin, g/dL, median (range)	11.0 (7.7–14.3)
≥10 g/dL	16 (67)
<10 g/dL	8 (33)
β2-microglobulin, mg/L, median (range)	3.6 (1.7–9.7)
≥3.5 mg/L	13 (54)
<3.5 mg/L	11 (46)
Number of medullary lesions, n (%)	
0	1 (4)
3–1 month	6 (25)
7–4 month	2 (8)
>7	15 (63)
Number of EMD, n (%)	
0	18 (75)
3–1 month	4 (17)
7–4 month	1 (4)
>7	1 (4)
Localization of EMD, n (%)	
Lymph node	3 (12)
Parenchymal organ	2 (8)
Soft tissue	1 (4)
SUV_{max}, median (range)	8.15 (3.81–39.14)
Localization of the hottest lesion, n (%)	
Medullary	22 (92)
Extramedullary	2 (8)
Comparison between DWMRI and 18F-FDG-PET/CT (n = 6), n (%)	
Number of DWI positive lesions > FDG avid lesions	2 (33)
Number of DWI positive lesions < FDG avid lesions	1 (17)
Number of DWI positive lesions = FDG avid lesions	3 (50)

18F-FDG-PET/CT—18F-fluorodeoxyglucose positron emission tomography/computed tomography; CKD-EPI—Chronic Kidney Disease Epidemiology Collaboration; eGFR—estimated glomerular filtration rate; DWI—diffusion-weighted imaging; DWMRI—diffusion-weighted magnetic resonance imaging; EMD—extramedullary disease; LDH—lactate dehydrogenase; NA—not available; SUV_{max}—maximum standardized uptake value.

3.3. Cytogenetics and Imaging Patterns of Relapse and Progression

We analyzed the link between cytogenetics and imaging patterns of relapse and progression, which were demonstrated in 18F-FDG PET/CT scans. Cytogenetics obtained at the last relapse/progression was available in 23 patients. High-risk cytogenetics, as determined by FISH, was present in eight (33%) patients, with four (17%), five (21%), one (4%) patients harboring del(17p), t(4;14), and t(14;16), respectively. Ten (42%) patients exhibited gain(1q21). Fifteen (63%) patients had standard-risk cytogenetics. EMD prevalence in patients with high-risk cytogenetics was slightly higher than that with standard-risk cytogenetics (2/8, 25% versus 3/15, 20%). In the patient with primary PCL and soft tissue EMD progression, we did not find any unfavorable cytogenetic alterations, such as t(4;14), del(17p), or gain(1q21), and the patient exhibited t(11;14). Among the three penta-refractory patients, two of them had hyperdiploid myeloma, and one patient displayed t(11;14) and gain(1q21).

We observed a significantly higher SUV_{max} in patients harboring del(17p) when compared with those without del(17p) (median SUV_{max} : 27.03 versus 6.04, $p = 0.025$, Figure 2A). Moreover, patients with high-risk cytogenetics showed a significantly higher SUV_{max} in comparison with those with standard-risk cytogenetics (median SUV_{max} : 12.80 versus 5.54, $p = 0.026$, Figure 2B). Furthermore, we observed no difference in SUV_{max} between patients with and without gain(1q21) ($p = 0.200$, figure not shown). Importantly, a high SUV_{max} of >15 indicated a significantly inferior PFS ($p = 0.01$, Figure 3A) and OS ($p = 0.0002$, Figure 3B) in our patients with RRMM.

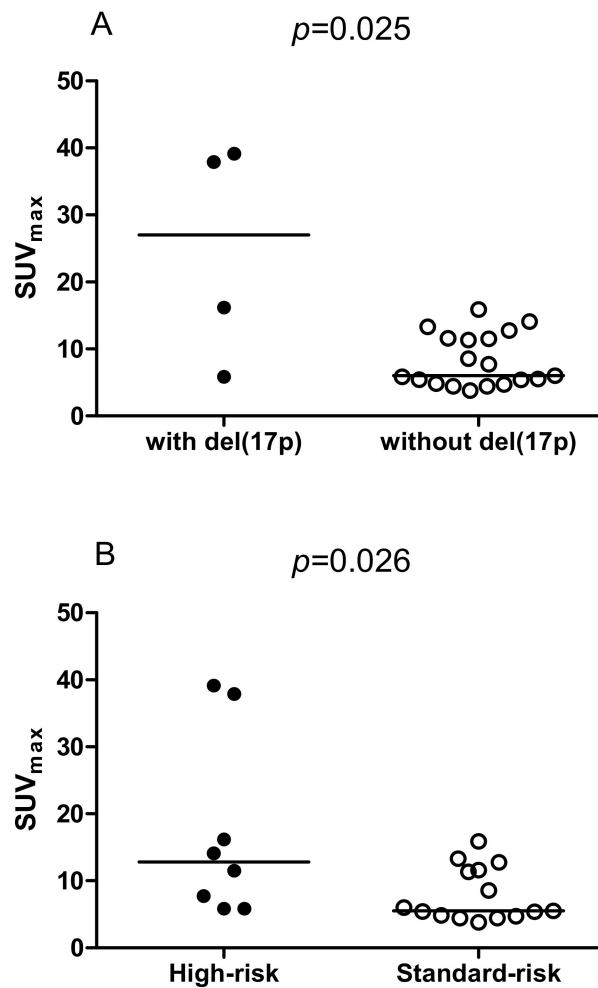


Figure 2. Link between cytogenetics and maximum standardized uptake value (SUV_{max}): (A) Patients with del(17p) ($n = 4$) showed a significantly higher SUV_{max} compared with those without del(17p) ($n = 19$) ($p = 0.025$). (B) High-risk cytogenetics, i.e., t(4;14), t(14;16), and del(17p) ($n = 8$) indicated a significantly higher SUV_{max} when compared with standard-risk cytogenetics ($n = 15$) ($p = 0.026$).

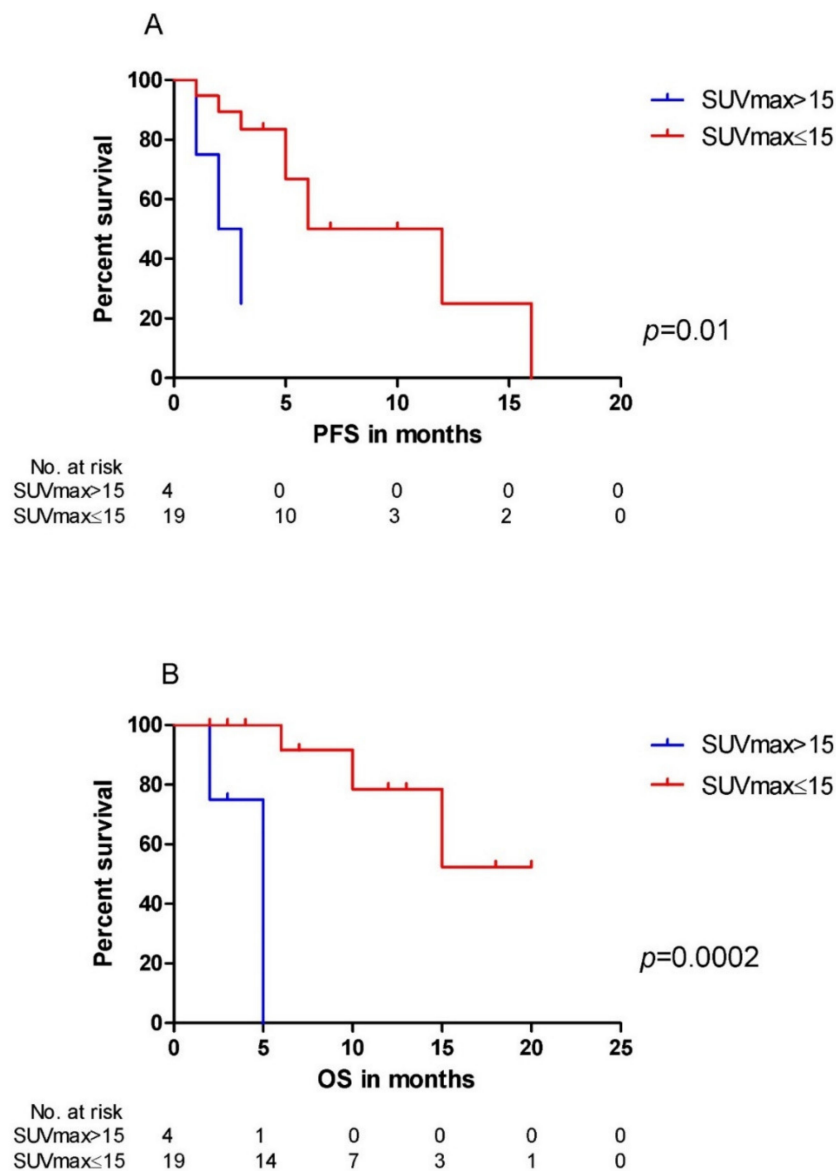


Figure 3. Maximum standardized uptake value (SUV_{max}) and survival: **(A)** Progression free survival (PFS) of patients with SUV_{max} >15 ($n = 4$) was significantly shorter than that in patients with SUV_{max} ≤15 ($n = 19$) ($p = 0.01$). **(B)** Patients with SUV_{max} >15 ($n = 4$) had a significantly inferior overall survival (OS) compared to those with SUV_{max} ≤15 ($n = 19$) ($p = 0.0002$).

3.4. WGS and Imaging Patterns of Relapse and Progression

To further elucidate the relationship between genomic alterations and imaging patterns, we also reviewed the data of WGS at the last relapse/progression, which were available in nine out of 24 patients. In these nine patients, WGS data could confirm structural changes within the genome, including translocations, amplifications, and deletions, which had been detected by FISH analysis at the last relapse/progression. Overall, t(14;16) and gain(1q21) were present in one (11%) and five (56%) patients, respectively. One (11%) patient exhibited del(17p). With regard to gene mutation status, KRAS represented the most frequently mutated gene in our cohort ($n = 4$, 44%), followed by NRAS ($n = 2$, 22%) mutation. WGS data and the patients' characteristics are presented in Table 3.

Notably, there was one female patient with biallelic TP53 alteration (patient No. 5 in Table 3). In this patient, a del(17p) was found by FISH analysis. The WGS data revealed a TP53 mutation

ENST00000269305.4:c.375 + 1G > T with a variant allele frequency (vaf) of 84% in one allele and a loss of the remaining allele through deletion chr17_p13.3_1::18986000_p11.2 (Figure 4A). At the last relapse/progression, this patient suffered from serological disease progression with EMD in lymph nodes. She received an allogeneic SCT as salvage therapy, and, two months later, this patient developed a new true EMD lesion in lymph node with excessive FDG uptake (Figure 4B). Interestingly, in 18F-FDG PET/CT scans, this patient also showed the highest SUV_{max}, which was much higher than the other eight patients (Table 3). This finding was consistent with our results demonstrated by FISH analysis that del(17p) indicated a significantly higher SUV_{max} at relapse/progression in 18F-FDG PET/CT scans in RRMM patients compared with those without del(17p).

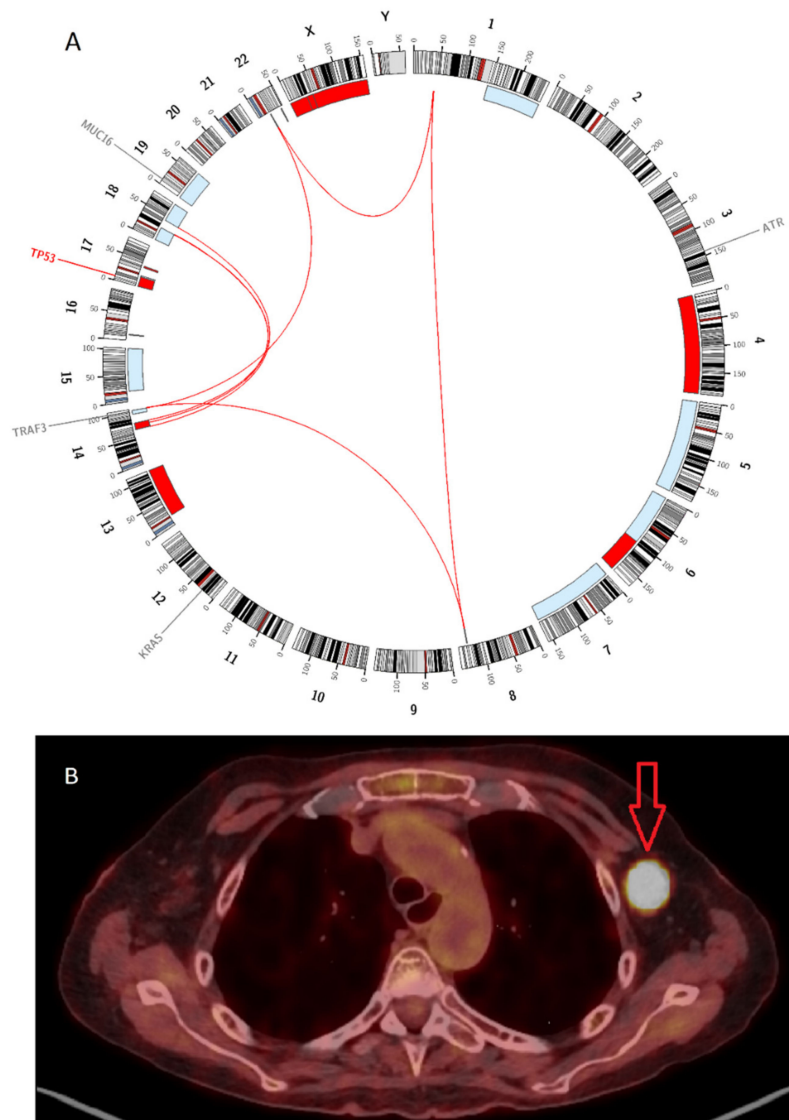


Figure 4. Whole-genome sequencing (WGS) and 18F-FDG PET/CT in the patient with biallelic *TP53* alteration (No. 5 in Table 3): (A) Circos plot demonstrated data of WGS, including copy number variations (CNV), structural variations (SV), and single nucleotide variations (SNV), at the last relapse. Gains and losses of >1 Mb are shown in blue and red, respectively. Interchromosomal reciprocal translocations with variant allele frequency (vaf) >0.1 are displayed by red lines inside the circle. Gene mutations (*TP53*) and variants (*ATR*, *KRAS*, *TRAF3*, and *MUC16*) are marked in red and grey, respectively. (B) True extramedullary disease (axillary lymph node) with excessive FDG uptake, as shown on 18F-FDG PET/CT scans. Biallelic *TP53* alteration might lead to aggressive tumor growth, e.g., development of extramedullary disease (EMD) and excessive FDG uptake.

Table 3. Whole-genome sequencing and imaging patterns in 18F-FDG PET/CT scans.

Patient	Gender	Age at Diagnosis	Subtype	Lines of Prior Therapy	Mutated Genes	High-Risk Structural Alterations	SUV _{max}	EMD	Size of the Largest EMD, cm	Localization of the Largest EMD
1	M	54	IgA Kappa	5	<i>KRAS</i>	None	5.4	No	/	/
2	F	75	IgG Kappa	3	<i>KRAS</i> , <i>CUL4B</i>	None	12.78	Yes	2.6	Lymph node
3	M	48	IgG Kappa	3	<i>BRAF</i>	None	4.44	No	/	/
4	M	78	IgG Kappa	1	None	None	8.58	No	/	/
5	F	60	IgG Kappa	7	<i>TP53</i>	del(17p), gain(1q21)	37.88	Yes	3.1	Lymph node
6	M	66	IgA Kappa	2	<i>KRAS</i> , <i>MUC16</i> , <i>NRAS</i> , <i>RRBP1</i> , <i>FAM46C</i>	gain(1q21)	11.36	No	/	/
7	F	64	IgA Kappa	8	<i>KRAS</i>	gain(1q21)	6.04	No	/	/
8	F	74	IgA Lambda	2	None	t(14;16), gain(1q21)	7.73	No	/	/
9	M	72	Kappa LC	1	<i>NRAS</i>	gain(1q21)	13.31	No	/	/

18F-FDG-PET/CT—18F-fluorodeoxyglucose positron emission tomography/computed tomography; EMD—extramedullary disease; F—female; LC—light chain; M—male; SUV_{max}—maximum standardized uptake value.

4. Discussion

We performed this pilot study utilizing 18F-FDG PET/CT to explore the potential link between cytogenetic/genomic characteristics and imaging patterns of relapse and progression in MM. To the best of our knowledge, this is the first study analyzing this link in patients with RRMM.

Overall, in our cohort, a high SUV_{max} of >15 on 18F-FDG PET/CT scans indicated significantly inferior PFS and OS in patients with relapsed or progressive MM. In 18F-FDG PET/CT, generally, SUV_{max} is a semi-quantitative parameter correlated with glucose uptake and metabolic or proliferative activity of the tumor [9]. So far, published data on the prognostic role of SUV_{max} in RRMM are still very limited [2]. Recently, in another study of Jamet *et al.*, SUV_{max} of >15.9 was identified as an independent negative prognostic factor for PFS [10] in patients with relapsed MM. In addition, Lapa *et al.* found that SUV_{max} of >18.57 was predictive for a shorter time to progression (TTP) in patients with MM relapse after autologous SCT [11]. In our study, we took a comparable cut-off value of SUV_{max} (>15), as already reported, and our results were in line with these previous studies. These findings underline the prognostic value of SUV_{max} on 18F-FDG PET/CT scans for RRMM patients.

As yet, little is known about the link between cytogenetics and semi-quantitative parameters in 18F-FDG PET/CT scans, such as SUV_{max} in RRMM patients. In our cohort, RRMM patients with high-risk cytogenetics, including del(17p), showed a significantly higher SUV_{max} in 18F-FDG PET/CT scans compared with those with standard-risk cytogenetics. More importantly, among the four patients with SUV_{max} of >15, three of them (3/4) showed del(17p) and, consequently, also high-risk cytogenetics. As reported by IMWG in the R-ISS in 2015, primary genetic events t(4;14), t(14;16) and secondary genetic abnormality del(17p) are known as negative prognostic factors in MM, and R-ISS is one of the most widely used prognostic models worldwide [8,12]. Additionally, in a study of Zamagni *et al.*, (1) high-risk cytogenetics, *i.e.*, del(17p) and t(4;14), and (2) the presence of lesions with SUV > 4.2 were identified as negative prognostic factors for PFS in NDMM [13]. At this point, our study demonstrated the prognostic values of high-risk cytogenetics and high SUV_{max} in RRMM and elucidated the link between both prognostic factors, suggesting that imaging parameters, such as SUV_{max}, might be a potential surrogate marker of cytogenetics in RRMM. Similar to previous studies, EMD was also enriched in patients with high-risk cytogenetics in our cohort [14,15]. However, these findings should be interpreted with caution due to the small patient population in our analysis. Altogether, the current study demonstrated that both SUV_{max} and cytogenetics, probably due to the potential link between both factors, were predictive for the survival outcome of RRMM patients.

In our cohort, WGS data revealed a patient with biallelic *TP53* alteration, in whom an extremely high SUV_{max} of 37.88 was presented by 18F-FDG PET/CT scans. *TP53* is a well-known tumor suppressor

gene, and its dysfunction is associated with various malignant diseases in humans [16]. In this patient, we detected a *TP53* mutation ENST00000269305.4:c.375 + 1G > T, which had been reported in ovarian cancer and breast cancer in the International Agency for Research on Cancer (IARC) *TP53* Mutation Database [17]. Currently, the role of this SNV is not fully understood. Mutations in this region could affect a splice site in intron 4 of *TP53* and might result in a frameshift and probably the loss of *TP53* function [18]. Thus, this SNV has been classified as a pathogenic variant in the Catalogue of Somatic Mutations in Cancers (COSMIC) database (Legacy Identifier: COSM69405). In addition, we observed a loss of the remaining *TP53* allele due to a large deletion chr17_p13.3_1::18986000_p11.2. Taken together, this patient presented a so-called double-hit *TP53* alteration, i.e., mutation plus deletion, which might result in a severe deficiency of *TP53* function. Interestingly, we observed the highest FDG uptake in an EMD lesion (SUV_{max} 37.88), indicating an extremely high metabolic and proliferative activity of EMD. Biallelic *TP53* alteration might correlate with aggressive behaviors of MM, e.g., development of EMD and excessive FDG uptake. This finding should be further evaluated in larger studies.

The current pilot study had several limitations: (1) In our study, we selected 18F-FDG PET/CT scans as a candidate parameter to elucidate the link between cytogenetics/genomics and imaging patterns in RRMM. While 18F-FDG clearly is the standard of reference tracer in nuclear imaging of MM, scan results might be influenced by different factors, such as expression levels of hexokinase-2 and glucose transporter, as well as hyperglycemia, and false-positive results due to infection, chronic inflammation, metallic implants, surgery, and fracture healing can occur [2,19–22]. In this context, the hexokinase-2 expression is increased in the HY and PR molecular subgroup [19]. In principle, additional semi-quantitative parameters, such as MTV and TLG, or PET/CT using other tracers, such as 11C-methionine [23,24] and 68Ga-Pentixafor [25,26], can also be used. A combination of different imaging methods might help to reduce the opportunities for bias. (2) Additional gene analysis of EMD lesions, if available, should also be performed to further evaluate the link between imaging patterns and special cytogenetic/genomic features of EMD [27]. (3) Our patients had received heterogeneous pretreatment, which might impact the clonal evolution and, consequently, also the genetic/genomic profile of MM cells. (4) As our pilot study was a retrospective study based on a limited number of patients, we did not perform multivariate survival analysis, and our findings should be interpreted with caution. Nevertheless, our findings have given insight into the biological background of imaging patterns in RRMM and have provided a rationale for further investigations.

5. Conclusions

In conclusion, this pilot study suggested a link between del(17p)/*TP53* alteration and FDG-uptake on FDG PET/CT scans in RRMM patients. Further larger studies are highly warranted at this point.

Supplementary Materials: The following are available online at <http://www.mdpi.com/2072-6694/12/9/2399/s1>, Supplementary Methods.

Author Contributions: Conceptualization, X.Z., K.M.K., L.R. and C.L.; Data curation, A.D., M.K., S.S., A.K.B., D.B. and C.L.; Formal analysis, X.Z., O.K., M.K., L.S. and J.M.; Investigation, X.Z., A.D., M.T., C.H. and C.L.; Methodology, A.D., M.T., C.H., S.K., L.S. and K.M.K.; Project administration, X.Z., M.K., H.E. and M.B.; Resources, L.H., O.K. and J.M.; Supervision, A.K.B., K.M.K., L.R., H.E. and C.L.; Validation, D.B.; Visualization, M.K. and S.K.; Writing—original draft, X.Z., A.D. and O.K.; Writing—review & editing, A.K.B., S.K., D.B., L.S., M.B., L.R., H.E. and C.L. All authors have read and agreed to the published version of the manuscript.

Funding: This publication was supported by the Open Access Publication Fund of the University of Wuerzburg.

Conflicts of Interest: All authors declare that they have no conflict of interest relevant to the submitted manuscript.

References

1. Robak, P.; Drozd, I.; Szemraj, J.; Robak, T. Drug resistance in multiple myeloma. *Cancer Treat. Rev.* **2018**, *70*, 199–208. [CrossRef] [PubMed]

2. Cavo, M.; Terpos, E.; Nanni, C.; Moreau, P.; Lentzsch, S.; Zweegman, S.; Hillengass, J.; Engelhardt, M.; Usmani, S.Z.; Vesole, D.H.; et al. Role of (18)F-FDG PET/CT in the diagnosis and management of multiple myeloma and other plasma cell disorders: A consensus statement by the International Myeloma Working Group. *Lancet Oncol.* **2017**, *18*, e206–e217. [[CrossRef](#)]
3. Stolzenburg, A.; Luckerath, K.; Samnick, S.; Speer, M.; Kneer, K.; Schmid, J.S.; Grigoleit, G.U.; Hofmann, S.; Beer, A.J.; Bunjes, D.; et al. Prognostic value of [(18)F]FDG-PET/CT in multiple myeloma patients before and after allogeneic hematopoietic cell transplantation. *Eur. J. Nucl. Med. Mol. Imaging* **2018**, *45*, 1694–1704. [[CrossRef](#)] [[PubMed](#)]
4. Mai, E.K.; Hielscher, T.; Kloth, J.K.; Merz, M.; Shah, S.; Hillengass, M.; Wagner, B.; Hose, D.; Raab, M.S.; Jauch, A.; et al. Association between magnetic resonance imaging patterns and baseline disease features in multiple myeloma: Analyzing surrogates of tumour mass and biology. *Eur. Radiol.* **2016**, *26*, 3939–3948. [[CrossRef](#)]
5. Rasche, L.; Angtuaco, E.J.; Alpe, T.L.; Gershner, G.H.; McDonald, J.E.; Samant, R.S.; Kumar, M.; Van Hemert, R.; Epstein, J.; Deshpande, S.; et al. The presence of large focal lesions is a strong independent prognostic factor in multiple myeloma. *Blood* **2018**, *132*, 59–66. [[CrossRef](#)]
6. McDonald, J.E.; Kessler, M.M.; Gardner, M.W.; Buros, A.F.; Ntambi, J.A.; Waheed, S.; van Rhee, F.; Zangari, M.; Heuck, C.J.; Petty, N.; et al. Assessment of Total Lesion Glycolysis by (18)F FDG PET/CT Significantly Improves Prognostic Value of GEP and ISS in Myeloma. *Clin. Cancer Res.* **2017**, *23*, 1981–1987. [[CrossRef](#)]
7. Rajkumar, S.V.; Harousseau, J.L.; Durie, B.; Anderson, K.C.; Dimopoulos, M.; Kyle, R.; Blade, J.; Richardson, P.; Orłowski, R.; Siegel, D.; et al. Consensus recommendations for the uniform reporting of clinical trials: Report of the International Myeloma Workshop Consensus Panel 1. *Blood* **2011**, *117*, 4691–4695. [[CrossRef](#)]
8. Palumbo, A.; Avet-Loiseau, H.; Oliva, S.; Lokhorst, H.M.; Goldschmidt, H.; Rosinol, L.; Richardson, P.; Caltagirone, S.; Lahuerta, J.J.; Facon, T.; et al. Revised International Staging System for Multiple Myeloma: A Report From International Myeloma Working Group. *J. Clin. Oncol.* **2015**, *33*, 2863–2869. [[CrossRef](#)]
9. Kinahan, P.E.; Fletcher, J.W. Positron emission tomography-computed tomography standardized uptake values in clinical practice and assessing response to therapy. *Semin. Ultrasound CT MR* **2010**, *31*, 496–505. [[CrossRef](#)]
10. Jamet, B.; Bailly, C.; Carlier, T.; Planche, L.; Touzeau, C.; Kraeber-Bodere, F.; Moreau, P.; Bodet-Milin, C. Added prognostic value of FDG-PET/CT in relapsing multiple myeloma patients. *Leuk. Lymphoma* **2019**, *60*, 222–225. [[CrossRef](#)]
11. Lapa, C.; Luckerath, K.; Malzahn, U.; Samnick, S.; Einsele, H.; Buck, A.K.; Herrmann, K.; Knop, S. 18 FDG-PET/CT for prognostic stratification of patients with multiple myeloma relapse after stem cell transplantation. *Oncotarget* **2014**, *5*, 7381–7391. [[CrossRef](#)] [[PubMed](#)]
12. Abe, Y.; Sunami, K.; Yamashita, T.; Ueda, M.; Takamatsu, H.; Narita, K.; Kobayashi, H.; Kitadate, A.; Takeuchi, M.; Matsue, K. Improved survival outcomes and relative youthfulness of multiple myeloma patients with t(4;14) receiving novel agents are associated with poorer performance of the revised international staging system in a real aging society. *Oncotarget* **2019**, *10*, 595–605. [[CrossRef](#)] [[PubMed](#)]
13. Zamagni, E.; Patriarca, F.; Nanni, C.; Zannetti, B.; Englara, E.; Pezzi, A.; Tacchetti, P.; Buttignol, S.; Perrone, G.; Brioli, A.; et al. Prognostic relevance of 18-F FDG PET/CT in newly diagnosed multiple myeloma patients treated with up-front autologous transplantation. *Blood* **2011**, *118*, 5989–5995. [[CrossRef](#)] [[PubMed](#)]
14. Besse, L.; Sedlarikova, L.; Greslikova, H.; Kupska, R.; Almasi, M.; Penka, M.; Jelinek, T.; Pour, L.; Adam, Z.; Kuglik, P.; et al. Cytogenetics in multiple myeloma patients progressing into extramedullary disease. *Eur. J. Haematol.* **2016**, *97*, 93–100. [[CrossRef](#)] [[PubMed](#)]
15. Rasche, L.; Bernard, C.; Topp, M.S.; Kapp, M.; Duell, J.; Wesemeier, C.; Haralambieva, E.; Maeder, U.; Einsele, H.; Knop, S. Features of extramedullary myeloma relapse: High proliferation, minimal marrow involvement, adverse cytogenetics: A retrospective single-center study of 24 cases. *Ann. Hematol.* **2012**, *91*, 1031–1037. [[CrossRef](#)]
16. Levine, A.J.; Momand, J.; Finlay, C.A. The p53 tumour suppressor gene. *Nature* **1991**, *351*, 453–456. [[CrossRef](#)]
17. Bouaoun, L.; Sonkin, D.; Ardin, M.; Hollstein, M.; Byrnes, G.; Zavadil, J.; Olivier, M. TP53 Variations in Human Cancers: New Lessons from the IARC TP53 Database and Genomics Data. *Hum. Mutat.* **2016**, *37*, 865–876. [[CrossRef](#)]
18. Baralle, D.; Baralle, M. Splicing in action: Assessing disease causing sequence changes. *J. Med. Genet.* **2005**, *42*, 737–748. [[CrossRef](#)]

19. Rasche, L.; Angtuaco, E.; McDonald, J.E.; Buros, A.; Stein, C.; Pawlyn, C.; Thanendrarajan, S.; Schinke, C.; Samant, R.; Yaccoby, S.; et al. Low expression of hexokinase-2 is associated with false-negative FDG-positron emission tomography in multiple myeloma. *Blood* **2017**, *130*, 30–34. [[CrossRef](#)]
20. Kitamura, S.; Yanagi, T.; Inamura-Takashima, Y.; Imafuku, K.; Hata, H.; Uehara, J.; Ishida, Y.; Otsuka, A.; Hirata, K.; Shimizu, H. Retrospective study on the correlation between 18-fluorodeoxyglucose uptake in positron emission tomography-computer tomography and tumour volume, cytological activity as assessed with Ki-67 and GLUT-1 staining in 10 cases of Merkel cell carcinoma. *J. Eur. Acad. Dermatol. Venereol.* **2018**, *32*, e285–e287. [[CrossRef](#)]
21. Martin, O.; Aissa, J.; Boos, J.; Wingendorf, K.; Latz, D.; Buchbender, C.; Gaspers, S.; Antke, C.; Sedlmair, M.; Antoch, G.; et al. Impact of different metal artifact reduction techniques on attenuation correction in 18F-FDG PET/CT examinations. *Br. J. Radiol.* **2020**, *93*, 20190069. [[CrossRef](#)] [[PubMed](#)]
22. Rabkin, Z.; Israel, O.; Keidar, Z. Do hyperglycemia and diabetes affect the incidence of false-negative 18F-FDG PET/CT studies in patients evaluated for infection or inflammation and cancer? A Comparative analysis. *J. Nucl. Med.* **2010**, *51*, 1015–1020. [[CrossRef](#)] [[PubMed](#)]
23. Lapa, C.; Garcia-Velloso, M.J.; Luckerath, K.; Samnick, S.; Schreder, M.; Otero, P.R.; Schmid, J.S.; Herrmann, K.; Knop, S.; Buck, A.K.; et al. (11)C-Methionine-PET in Multiple Myeloma: A Combined Study from Two Different Institutions. *Theranostics* **2017**, *7*, 2956–2964. [[CrossRef](#)] [[PubMed](#)]
24. Lapa, C.; Knop, S.; Schreder, M.; Rudelius, M.; Knott, M.; Jorg, G.; Samnick, S.; Herrmann, K.; Buck, A.K.; Einsele, H.; et al. 11C-Methionine-PET in Multiple Myeloma: Correlation with Clinical Parameters and Bone Marrow Involvement. *Theranostics* **2016**, *6*, 254–261. [[CrossRef](#)] [[PubMed](#)]
25. Lapa, C.; Schreder, M.; Schirbel, A.; Samnick, S.; Kortum, K.M.; Herrmann, K.; Kropf, S.; Einsele, H.; Buck, A.K.; Wester, H.J.; et al. [(68)Ga]Pentixafor-PET/CT for imaging of chemokine receptor CXCR4 expression in multiple myeloma—Comparison to [(18)F]FDG and laboratory values. *Theranostics* **2017**, *7*, 205–212. [[CrossRef](#)]
26. Pan, Q.; Cao, X.; Luo, Y.; Li, J.; Feng, J.; Li, F. Chemokine receptor-4 targeted PET/CT with (68)Ga-Pentixafor in assessment of newly diagnosed multiple myeloma: Comparison to (18)F-FDG PET/CT. *Eur. J. Nucl. Med. Mol. Imaging* **2020**, *47*, 537–546. [[CrossRef](#)]
27. Rasche, L.; Chavan, S.S.; Stephens, O.W.; Patel, P.H.; Tytarenko, R.; Ashby, C.; Bauer, M.; Stein, C.; Deshpande, S.; Wardell, C.; et al. Spatial genomic heterogeneity in multiple myeloma revealed by multi-region sequencing. *Nat. Commun.* **2017**, *8*, 268. [[CrossRef](#)]



© 2020 by the authors. Licensee MDPI, Basel, Switzerland. This article is an open access article distributed under the terms and conditions of the Creative Commons Attribution (CC BY) license (<http://creativecommons.org/licenses/by/4.0/>).